Letter

Spectral detuning of relativistic surface harmonics

Elkana Porat,[1,2,3,*] Itamar Cohen,[1,2] Assaf Levanon,[1,2] and Ishay Pomerantz[1,2]
[1]*The School of Physics and Astronomy, Tel Aviv University, Tel Aviv 69978, Israel*
[2]*Center for Light-Matter Interaction, Tel Aviv University, Tel Aviv 69978, Israel*
[3]*Department of Applied Physics, Soreq Nuclear Research Center, Yavne 81800, Israel*

(Received 10 February 2022; accepted 29 April 2022; published 16 May 2022)

Relativistic surface harmonics driven by high-intensity lasers are considered a promising future light source, as their bandwidth and brightness are scalable with the driving laser power. Typically, the emission frequencies of these sources are limited to integer multiples of the laser fundamental frequency. In this Letter, we describe how the generation dynamics of these harmonics may enable spectral detuning of their frequencies. A dent in the plasma surface driven by the radiation pressure of the laser field grows during the interaction and varies the harmonic beam divergence. When a temporal chirp is added to the driving laser pulse, different instantaneous fundamental frequencies drive the harmonic beam to different cone angles, resulting in an overall spectral detuning of the high harmonics beam. We present experimental measurements of the dependence of the spectral detuning on the temporal chirp of the driving pulse. We show how these results are reproduced by our model, and conclude with its predictions for higher intensity laser systems.

DOI: 10.1103/PhysRevResearch.4.L022036

The interaction of an ultraintense laser field with a sharp-gradient plasma surface forms a relativistic optical element known as plasma mirror (PM) [1]. Relativistic PM dynamics are manifested by the emission of attosecond bursts of energetic electrons and coherent extreme ultraviolet (EUV) light. Bright ultrashort EUV pulses are of great interest to ultrafast science because they are a prerequisite for many applications, including attosecond spectroscopy [2], biological imaging [3], and material sciences [4].

The EUV emission spectrum features a comb of high-order harmonics (HHs) of the fundamental frequency. These so-called surface harmonics originate from two distinct types of plasma dynamics: At moderate laser intensities, of over $I\lambda^2 > 10^{16}\ \mathrm{W\,cm^{-2}}\,\mu\mathrm{m}^2$ with λ being the laser wavelength, HHs are generated by a subrelativistic process known as coherent wake emission (CWE) [5]. Beyond the relativistic threshold of about $I\lambda^2 > 10^{18}\ \mathrm{W\,cm^{-2}}\,\mu\mathrm{m}^2$, the relativistic oscillating mirror (ROM) [6] and the coherent synchrotron emission [7,8] mechanisms prevail. The promising applicative property of these latter processes is their intensity-scalable generation efficiency and bandwidth [9].

For some applications, however, the ability to tune the emission frequency around the narrow band of an individual harmonic order is a prerequisite. In EUV spectroscopy [10,11], the ability to tune the emission frequency allows probing of specific atomic or molecular resonances. In lensless imaging, multispectral illumination provides direct information about the chemical composition of the interrogated sample [12].

High-order harmonic generation (HHG) in gas, which is inherently limited in scaling to ultrahigh laser intensities, may be easily manipulated to detune the harmonic frequency by, e.g., the introduction of a temporal chirp to the pulse [13], or the addition of an auxiliary pulse to induce optical parametric generation [14] or interference [15] in the gas target. Another means to detune the frequency of HHG in gaseous media is to simply shift the frequency of the fundamental IR pulse [16]. This approach, however, is not straightforward for HHG from relativistic PMs because multi-terrawatt (TW) laser systems are typically limited to amplification around the central emission wavelength of a limited selection of high-gain amplifying media. For CWE, in which the emission phase is highly dependent on the instantaneous laser intensity, introduction of a temporal chirp results in spectral detuning [5,17].

A key aspect governing the emission properties of relativistic plasma surfaces is the denting of a plasma surface under the radiation pressure of the intense laser field [18]. The induced surface curvature results in strong focusing of the HH beam near the surface and increases its far-field divergence. This feature may be either mitigated [19,20] or employed to achieve unprecedented light intensities [21,22]. Here we demonstrate utilizing this transient plasma dent to enhance the emission of a specific instantaneous frequency of a chirped laser pulse.

The displacement of a critical plasma surface under the influence of an ultraintense laser field may be expressed as [23]

$$\delta_x = -L\ln\left(1 + 2\eta_i + \eta_e + \eta_i^2\right), \tag{1}$$

where L is the plasma scale length, and η_e and η_i are functions of the local normalized field amplitude $a_L(r,t)$ which

*elkanaporat@mail.tau.ac.il

represent the electronic and ionic contributions to the surface displacement, respectively [18]:

$$\eta_i(r,t) = \frac{c\Pi_0}{2L\cos\theta}\int_{t_r}^{t} a_L(r,t')\,dt',$$
$$\eta_e(r,t) = a_L(r,t)\frac{\lambda}{\pi L(1+\sin\theta)}. \quad (2)$$

Here c is the speed of light, θ is the laser's angle of incidence, and $\Pi_0 = \sqrt{R_p Z m_e}\cos\theta/2Am_p$, where $R_p \sim 0.7$ is the plasma reflection coefficient [18], Z and A are the charge and mass numbers of the plasma ions, respectively, having $Z/A = 2$ for fully ionized silica, and m_e and m_p are the electron and proton masses. In the regime of weakly relativistic laser intensity ($a_L \gtrsim 1$), the plasma denting is dominated by the ions displacement, monotonically increasing during the irradiation. We note that the plasma scale length, incorporated in Eqs. (1) and (2), can generally vary in space, depending on the spatial profile of the precursor light that drove the plasma expansion [24].

The dependence of L on the laser intensity is crucial for capturing the emission dynamics of relativistic plasma surfaces. Because the ion-acoustic velocity dependence on the hot electron temperature T_e is given by $C_s = \sqrt{ZT_e/Am_p}$ [25], it follows that $L \propto \sqrt{T_e}$. The electron temperature in turn is expected to be proportional to the absorbed laser intensity, and therefore to scale as $T_e \propto I_{\rm abs} \propto I_L^{\alpha}$. Finally we find

$$L(\boldsymbol{r}) \propto a_L^{\alpha}. \quad (3)$$

The values of the scaling parameter α were found to cover a wide range, from $\alpha \approx 1/3$ in picosecond laser irradiation of thick solids [26], to $\alpha \approx 1.1$ in high contrast femtosecond laser irradiation [27], and to $\alpha = 3/2$ in Brunel's theory [28]. Considering the high sensitivity of α to the precursor light profile, its value is kept as a free parameter in our analysis.

Both the expansion of the plasma and the denting under radiation pressure affect the reflecting plasma surface depth, which sets the amount of excess phase introduced to the reflected HH beam [23]:

$$\varphi_x = 2k_H\cos\theta\left\{L(\boldsymbol{r})\left[\ln\left(\frac{n_{e0}}{n_c}\right) - 1\right] + \delta_x(\boldsymbol{r},t)\right\}, \quad (4)$$

where $k_H = 2\pi H/\lambda$ is the Hth harmonic wave number, n_c the critical plasma density, and n_{e0} the electron density at the head of the density ramp.

Temporal variations of φ_x induce a Doppler shift of

$$\delta\omega_D = \frac{\partial}{\partial t}\varphi_x(r=0,t), \quad (5)$$

while spatial variations of φ_x modify the far-field divergence of the HH beam. For a laser tightly focused to a spot of radius w_L, the spatial phase variations are quantified by the normalized focusing parameter Ψ:

$$\Psi \equiv \frac{w_L^2}{\lambda R} = \frac{w_L^2}{H}\frac{\partial^2}{\partial r^2}\varphi_x(r=0,t), \quad (6)$$

where R is the phase front's radius of curvature of the HH beam. The normalized far-field divergence of the H harmonic

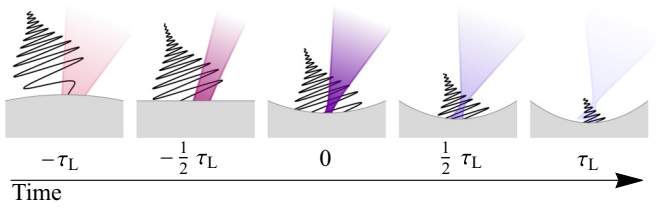

FIG. 1. Cartoon depiction of the emission dynamics leading to spectral detuning of a HH beam. The transverse component of a chirped laser pulse is illustrated in black. The relative average HH emission frequency is indicated in a red-to-blue color palette. Five temporal snapshots show how the evolution of the plasma surface curvature under the radiation pressure of the laser field modifies the HH emission cone angle, maximizing the emission brightness of a specific frequency-shifted harmonic.

is then [29]

$$\theta_H/\theta_L = \frac{w_L}{Hw_H}\sqrt{1+\left[2\pi H\left(\frac{w_H}{w_L}\right)^2\Psi\right]^2}, \quad (7)$$

where θ_L is the cone angle of the incident laser, and w_H is the source radius of the Hth harmonic. Assuming a nearly Gaussian focal spot, the source radius is closely related to the intensity scaling of the HH beam:

$$I_H \propto I_L^q, \quad w_L/w_H \approx \sqrt{q}, \quad (8)$$

through the scaling parameter q, whose value is found to be $q \approx 4$ [18,30].

When a temporal chirp is introduced to the driving laser pulse, the time-dependent divergence of the HH beam results in detuning of its peak spectral brightness. This idea is depicted in Fig. 1, which illustrates snapshots of a temporally chirped pulse incident on a PM surface. The transverse component of the laser field is plotted in black. The plasma surface, initially convex because of preexpansion, curves in under the radiation pressure of the laser field. At a given instant, the surface flattens and sets a minimal divergence to the instantaneous frequency of the HH beam.

Figure 2 shows the instantaneous intensity (a) and frequency shift (b) of a $\xi = -2$ chirped laser pulse. Here the dimensionless chirp parameter ξ is defined by $\tau_L = \tau_0\sqrt{1+\xi^2}$, where τ_L and τ_0 are the chirped and compressed pulse durations, respectively. The far-field divergence of the HH beam, calculated using Eq. (7) and shown in Fig. 2(c), becomes minimal when the plasma surface flattens under the radiation pressure of the laser field. The HH beam brightness is inversely proportional to the emission solid angle $d\Omega \propto \theta_H^2$. Thus, the peak of I_H is shifted in time with respect to I_L toward times of smaller divergence, as seen in Fig. 2(d). Because the driving laser is chirped, this time shift maximizes a specific instantaneous spectral component, detuned from the fundamental harmonic frequency. The resulting spectral shift for temporal chirps in the range of $-4 < \xi < 4$ is plotted in Fig. 2(e).

We carried out experiments using a 20 TW, 800 nm central wavelength laser system at Tel Aviv University. A key challenge for HHG from PMs are the stringent requirements for the temporal contrast of the laser [31]. Traditionally,

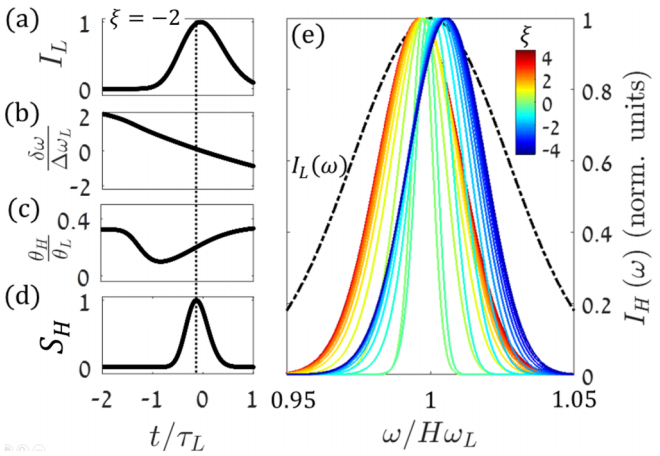

FIG. 2. Calculated spectral detuning of HH emission from a relativistic plasma surface, irradiated with a temporally chirped Gaussian laser pulse. (a) The instantaneous intensity and (b) frequency shift of a $\xi = -2$ chirped IR pulse, where $\Delta\omega_L$ is the bandwidth of the driving laser. (c) The instantaneous divergence and (d) far-field brightness of the reflected HH beam. The evolving HH beam divergence shifts its peak brightness (dashed line) to earlier times with respect to I_L. This shift maps a specific instantaneous frequency and results in spectral detuning. (e) The overall resulting spectral shifts for different values of the dimensionless chirps. The driving laser spectrum is shown in dash-dotted black.

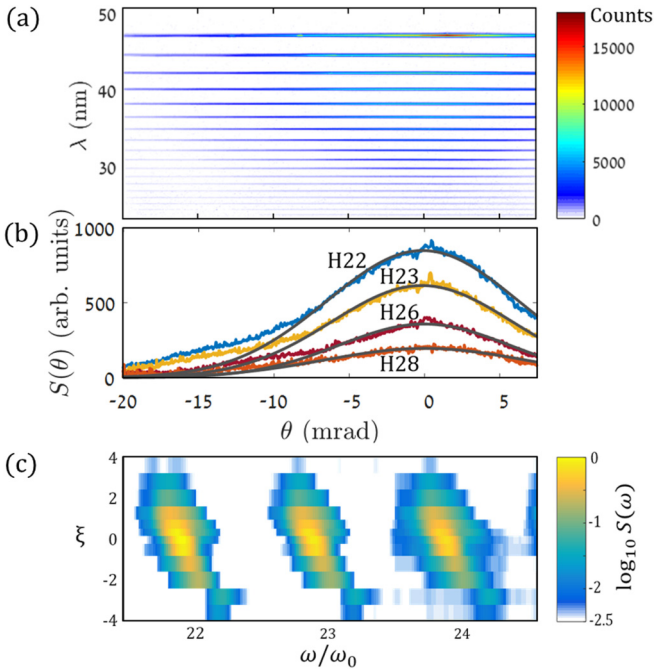

FIG. 3. (a) Typical raw spectrogram obtained by the irradiation of a PM with a $\xi = 0$, $a_0 = 2.2$ laser pulse, featuring HH emission orders from H17 to H34, which are well beyond the CWE cutoff frequency. (b) Angular profiles of several HH orders demonstrating the extraction of their angular divergence by fitting to a Gaussian form (black). (c) Spatially integrated spectra of H22–H24, taken at different laser chirps. The colormap is in logarithmic scale, normalized to the peak value at $\xi = 0$.

postcompression contrast enhancement in the form of an ultrafast optical switch is used. This solution, however, increases experiment complexity and lowers the available pulse energy on target. The work presented here was made possible by a newer generation high-power laser technology, with a front end based on picosecond optical parametric chirped pulse amplification [32]. A pristine temporal contrast, better than 10^{10}, is achieved up to $t = -40$ ps, and 10^6 up to $t = -1.4$ ps [24]. The spectral bandwidth of the amplified beam is 5.5% FWHM. An acousto-optic programmable dispersive filter [33] at the laser front end is used to achieve a nearly Fourier transform limited pulse duration of 30 fs of the fully amplified beam.

In these experiments, we introduced a controlled temporal chirp to the pulse by adjusting the distance between the two compressor gratings, using a motorized stage with absolute accuracy of better than 10 μm. The pulse duration used to calculate ξ was inferred from the grating separation and was verified against second-order single-shot autocorrelator measurements.

The laser beam was focused using a 16.3 cm focal length off-axis parabolic mirror onto a polished glass substrate with an angle of incidence of 55°. Before focusing, the beam is apertured to 3.2 cm diameter, which results in a focal spot size of 4.7 μm (FWHM) corresponding to a peak intensity of 1.05×10^{19} W cm^{-2} ($a_0 \approx 2.2$). We measured the emitted EUV radiation using a grazing-incidence flat-field EUV spectrometer, with a 4 megapixel charge-coupled device. The spectrometer was positioned in the reflection direction, 100 cm downstream from the target. A 200-nm-thick Al foil was placed at the entrance to the spectrometer to block visible light. We used the second-order diffraction of the aluminium L edge at $\lambda_{\text{Al-}L} \approx 17.05$ nm to calibrate the spectrometer to within 0.3% accuracy.

A typical EUV spectrogram obtained by irradiation with laser parameters of $\xi = 0$, $a_0 \approx 2.2$ is shown in Fig. 3(a). Harmonic orders in the range of $17 < H < 34$ are clearly observed, with a spectral single harmonic bandwidth of $\Delta\omega_H/\omega_H \approx 0.5\%$ (FWHM). The angular distribution of several HH orders is shown in Fig. 3(b), with a fit to Gaussian form. The harmonic orders above the CWE cutoff ($H > 20$) present similar divergence of 14.5 ± 0.8 mrad (FWHM), corresponding to a normalized divergence of $\theta_H/\theta_L \approx 0.2$.

HH spectrograms were recorded for laser pulses with temporal chirps in the range of $-4 < \xi < 4$. The spatially integrated spectra of harmonics H22–H24 are shown in Fig. 3(c) for different values of ξ. The spectral detuning of each harmonic toward blue (red), with negative (positive) chirp values is evident. The angular divergence of the HH beam is found to be independent of the chirp and within a shot-to-shot fluctuation of $\Delta\theta_H/\theta_H = 14\%$.

Our model, given by Eqs. (4)–(8), predicts the divergence, spectral detuning, and brightness of the HH beam. To evaluate these observables, we write the brightness of the Hth harmonic as

$$S_H(t) = \theta_H^{-2}\left|I_L^{q/2} e^{-iH(\omega_L+\Delta\omega_D)t}\right|^2. \tag{9}$$

$I_L(t)$, $\theta_H(t)$, and the laser frequency $\omega_L(t)$ are all instantaneous quantities. A temporal chirp is introduced to the pulse by addition of a compressor grating separation Δ,

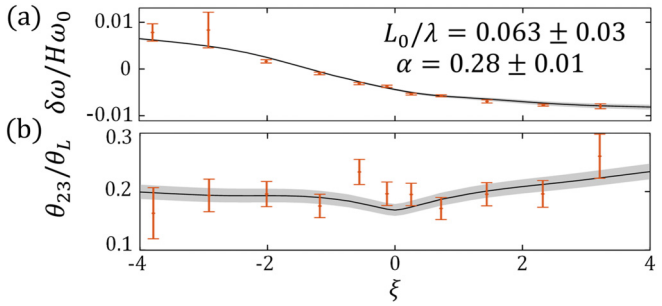

FIG. 4. Experimental results (red) and fitted model (black) for the (a) spectral detuning, averaged over H22–H26, and (b) normalized angular divergence of H23, plotted vs the amount of temporal chirp. In both panels, solid lines and shaded areas represent the fitted model with $\alpha = 0.28 \pm 0.01$, $L_0/\lambda = 0.063 \pm 0.03$.

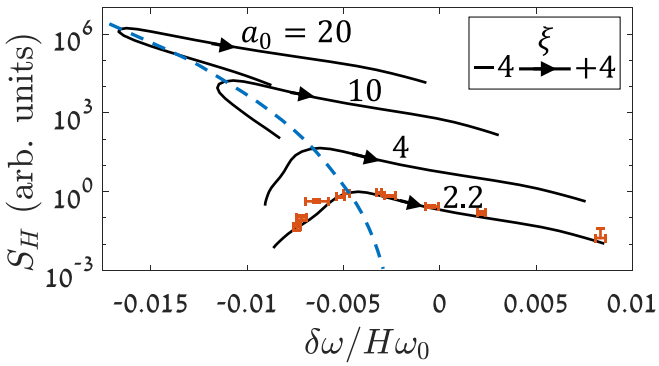

FIG. 5. Integrated HH brightness vs the average spectral detuning. The measured values of this work ($a_0 = 2.2$) are shown in red. Model calculations for different laser field strengths are plotted in black. Each curve is calculated for a temporal chirp range of $-4 < \xi < 4$. The amount of Doppler redshift for fully compressed pulses is shown in dashed blue, to indicate its role in the overall spectral detuning.

introducing second- and third-order spectral dispersion terms $\phi_2(\Delta), \phi_3(\Delta)$ [34]. The chirped instantaneous intensity is then given by

$$I_L(t) \propto \left|\mathcal{F}^{-1}\left\{\tilde{I}_L^{1/2}(\omega)e^{-i(\phi_2/2)(w-w_0)^2 - i(\phi_3/6)(w-w_0)^3}\right\}\right|^2. \quad (10)$$

We model the laser power spectrum $\tilde{I}_L$ as a smooth functional form

$$\tilde{I}_L(\omega) = \frac{1}{2}\left[1 + \cos\left(\pi\frac{\omega-\omega_0}{\Delta\omega}\right)\right]\Theta(\Delta\omega - |\omega-\omega_0|), \quad (11)$$

which reproduces the finite bandwidth $\Delta\omega$ of a realistic high-power laser beam around a central frequency ω_0. The second-order spectral phase can be related to ξ using Eqs. (10) and (11) giving

$$\xi \approx -0.31\Delta\omega^2\phi_2 + \mathrm{erf}(0.22\Delta\omega^2\phi_2). \quad (12)$$

With this machinery, the time-averaged divergence and frequency-averaged spectral detuning of the HH beam are given by

$$\langle\theta_H\rangle = \frac{\int_{-\infty}^{\infty}\theta_H(t)S_H(t)dt}{\int_{-\infty}^{\infty}S_H(t)dt}, \quad \langle\delta\omega\rangle = \frac{\int_{-\infty}^{\infty}\omega\tilde{S}_H(\omega)d\omega}{\int_{-\infty}^{\infty}\tilde{S}_H(\omega)d\omega} - H\omega_0, \quad (13)$$

where $\tilde{S}_H(\omega) = \mathcal{F}\{S_H(t)\}$ is the power spectrum of the HH beam.

The values of these two observables, measured over a range of temporal chirps, are shown in Fig. 4. The spectral detuning values in (a), representing the average of H22–H26, are shown with their standard deviation errors. Not shown is an additional overall systematic frequency calibration uncertainty of ±0.3%. The normalized angular divergence values in (b) are for H23, and their error bars reflect a ±1.5 μm uncertainty in the target surface position along the focal position, which propagates into w_L in Eq. (7).

We fitted our model to both data sets simultaneously, leaving the plasma scale length at the beam center, $L_0 \equiv L(\boldsymbol{r} = 0)$, and the intensity scaling exponent α as free parameters. The solid lines in Fig. 4 represent best-fit results, with the uncertainties represented by the gray bands. The value of the absorbed laser intensity scaling coefficient was found to be $\alpha = 0.28 \pm 0.09$, consistent with the empirically measured value [26].

The fitted plasma scale length, found to be $L_0/\lambda = 0.063 \pm 0.03$, is just above the threshold for the onset of ROM [35,36]. This should be expected in our experimental scenario, where the initial scale length was not optimized by an auxiliary prepulse [37]. For the laser intensity and temporal contrast in these experiments, plasma formation initiates at $t \approx -1.4$ ps. For this plasma expansion duration, L_0 is in good agreement with the literature [35]. To interpret the trend of the curve in Fig. 4(a), we note that Eq. (2) predicts the electronic and ionic contributions to the surface displacement to scale with laser pulse duration as $\eta_e \propto 1/\sqrt{\tau_L}$ and $\eta_i \propto \sqrt{\tau_L}$, respectively. For a small amount of chirp $|\xi| \lesssim 2$, these scalings counteract keeping δ_x roughly constant, making the spectral detuning nearly linear in ξ. By contrast, for large amounts of temporal chirps, $|\xi| \gtrsim 2$, the quadratic term η_i^2 in Eq. (1) becomes dominant, giving

$$\delta_x \approx L\eta_i^2 \propto \tau_L \quad (14)$$

bringing the amount of spectral detuning to saturation.

The relative HH brightness for different amounts of spectral detuning is presented in Fig. 5. The model prediction, calculated with the L_0 and α values found above without additional fitting, is plotted in black. The penalty for introducing a temporal chirp and thereby reducing the laser intensity is evident in the logarithmic drop of the HH beam brightness at high spectral shifts.

The predicted HH brightness for laser intensities up to $a_0 = 20$ is also presented in Fig. 5. The plasma scale length is predicted using Eq. (8), $L(a_0) = L_0(a_0/2.2)^\alpha$, for the same L_0 and α values. As the laser field is increased, the plasma dent grows faster because of stronger radiation pressure and longer plasma scale length. For increased laser intensities, the Doppler redshift becomes the dominant contribution to the spectral detuning, finally overcoming the temporal chirp contribution, thus presenting multivalued curves. This is demonstrated by the dashed blue line, which is a direct calculation of the Doppler shift using Eq. (5).

In this Letter, we demonstrated fine manipulation of the emission spectrum of HH beams by introducing a temporal

chirp to the driving laser pulse. A straightforward model of these dynamics reproduced the dependence of the two observables, $\delta\omega_0$ and θ_L, on the temporal chirp, with two free parameters, L_0 and α. An important future extension of this work would be a direct measurement of the plasma scale length before the main laser interaction, using, e.g., time-resolved frequency- or spatial-domain interferometry [38,39]. Direct measurement of the laser absorption scaling coefficient α is challenging, but values that were obtained from fitting the data may be validated using numeric simulations.

Another instructive extension of this study would be the introduction of a richer spectral phase control using, e.g., an acusto-optical modulator. In this scenario, Eq. (9) would be modified to account for the full details of the spectral phase, which preferably will be also measured directly, using, e.g., a FROG [40] or a SRSI [41].

We acknowledge the support by the Pazy Foundation, Grant No. 27707241, and by the Zuckerman STEM Leadership Program.

[1] B. Dromey, S. Kar, M. Zepf, and P. Foster, The plasma mirror: A subpicosecond optical switch for ultrahigh power lasers, Rev. Sci. Instrum. **75**, 645 (2004).

[2] P. H. Bucksbaum, The future of attosecond spectroscopy, Science **317**, 766 (2007).

[3] A. P. Mancuso, T. Gorniak, F. Staier, O. M. Yefanov, R. Barth, C. Christophis, B. Reime, J. Gulden, A. Singer, M. E. Pettit *et al.*, Coherent imaging of biological samples with femtosecond pulses at the free-electron laser FLASH, New J. Phys. **12**, 035003 (2010).

[4] S. Mathias, H. C. Kapteyn, and M. M. Murnane, Ultrafast material science probed using coherent x-ray pulses from high-harmonic generation, in *Ultrafast Nonlinear Optics* (Springer International Publishing, Heidelberg, 2013), Chap. 7, pp. 149–175.

[5] F. Quéré, C. Thaury, P. Monot, S. Dobosz, P. Martin, J.-P. Geindre, and P. Audebert, Coherent Wake Emission of High-Order Harmonics from Overdense Plasmas, Phys. Rev. Lett. **96**, 125004 (2006).

[6] B. Dromey, M. Zepf, A. Gopal, K. Lancaster, M. S. Wei, K. Krushelnick, M. Tatarakis, N. Vakakis, S. Moustaizis, R. Kodama, M. Tampo, C. Stoeckl, R. Clarke, H. Habara, D. Neely, S. Karsch, and P. Norreys, High harmonic generation in the relativistic limit, Nat. Phys. **2**, 456 (2006).

[7] D. an der Brügge and A. Pukhov, Enhanced relativistic harmonics by electron nanobunching, Phys. Plasmas **17**, 033110 (2010).

[8] B. Dromey, S. Rykovanov, M. Yeung, R. Hörlein, D. Jung, D. Gautier, T. Dzelzainis, D. Kiefer, S. Palaniyppan, R. Shah *et al.*, Coherent synchrotron emission from electron nanobunches formed in relativistic laser–plasma interactions, Nat. Phys. **8**, 804 (2012).

[9] M. R. Edwards and J. M. Mikhailova, The x-ray emission effectiveness of plasma mirrors: Reexamining power-law scaling for relativistic high-order harmonic generation, Sci. Rep. **10**, 5154 (2020).

[10] A. L'Huillier, D. Descamps, A. Johansson, J. Norin, J. Mauritsson, and C.-G. Wahlström, Applications of high-order harmonics, Eur. Phys. J. D **26**, 91 (2003).

[11] A. Cingöz, D. C. Yost, T. K. Allison, A. Ruehl, M. E. Fermann, I. Hartl, and J. Ye, Direct frequency comb spectroscopy in the extreme ultraviolet, Nature (London) **482**, 68 (2012).

[12] D. A. Shapiro, Y.-S. Yu, T. Tyliszczak, J. Cabana, R. Celestre, W. Chao, K. Kaznatcheev, A. D. Kilcoyne, F. Maia, S. Marchesini *et al.*, Chemical composition mapping with nanometre resolution by soft x-ray microscopy, Nat. Photonics **8**, 765 (2014).

[13] J. Zhou, J. Peatross, M. M. Murnane, H. C. Kapteyn, and I. P. Christov, Enhanced High-Harmonic Generation Using 25 fs Laser Pulses, Phys. Rev. Lett. **76**, 752 (1996).

[14] M. Gaarde, P. Antoine, A. Persson, B. Carré, A. L'Huillier, and C.-G. Wahlström, High-order tunable sum and difference frequency mixing in the XUV region, J. Phys. B: At., Mol. Opt. Phys. **29**, L163 (1996).

[15] V. Schuster, V. Hilbert, R. Klas, C. Liu, M. Tschernajew, B. Bernhardt, J. Rothhardt, and J. Limpert, Agile spectral tuning of high order harmonics by interference of two driving pulses, Opt. Express **29**, 22117 (2021).

[16] M. Wünsche, S. Fuchs, S. Aull, J. Nathanael, M. Möller, C. Rödel, and G. G. Paulus, Quasi-supercontinuum source in the extreme ultraviolet using multiple frequency combs from high-harmonic generation, Opt. Express **25**, 6936 (2017).

[17] A. Borot, A. Malvache, X. Chen, A. Jullien, J.-P. Geindre, P. Audebert, G. Mourou, F. Quéré, and R. Lopez-Martens, Attosecond control of collective electron motion in plasmas, Nat. Phys. **8**, 416 (2012).

[18] H. Vincenti, S. Monchocé, S. Kahaly, G. Bonnaud, P. Martin, and F. Quéré, Optical properties of relativistic plasma mirrors, Nat. Commun. **5**, 3403 (2014).

[19] J. Gao, B. Li, F. Liu, Z.-Y. Chen, M. Chen, X. Ge, X. Yuan, L. Chen, Z. Sheng, and J. Zhang, Divergence control of relativistic harmonics by an optically shaped plasma surface, Phys. Rev. E **101**, 033202 (2020).

[20] H. Kallala, F. Quéré, and H. Vincenti, Techniques to generate intense isolated attosecond pulses from relativistic plasma mirrors, Phys. Rev. Research **2**, 043007 (2020).

[21] H. Vincenti, Achieving Extreme Light Intensities using Optically Curved Relativistic Plasma Mirrors, Phys. Rev. Lett. **123**, 105001 (2019).

[22] L. Chopineau, A. Denoeud, A. Leblanc, E. Porat, P. Martin, H. Vincenti, and F. Quéré, Spatio-temporal characterization of attosecond pulses from plasma mirrors, Nat. Phys. **17**, 968 (2021).

[23] A. Leblanc, S. Monchocé, H. Vincenti, S. Kahaly, J.-L. Vay, and F. Quéré, Spatial Properties of High-Order Harmonic Beams from Plasma Mirrors: A Ptychographic Study, Phys. Rev. Lett. **119**, 155001 (2017).

[24] E. Porat, H. Yehuda, I. Cohen, A. Levanon, and I. Pomerantz, Diffraction-limited coherent wake emission, Phys. Rev. Research **3**, L032059 (2021).

[25] S. Gitomer, R. Jones, F. Begay, A. Ehler, J. Kephart, and R. Kristal, Fast ions and hot electrons in the laser–plasma interaction, Phys. Fluids **29**, 2679 (1986).

[26] F. Beg, A. Bell, A. Dangor, C. Danson, A. Fews, M. Glinsky, B. Hammel, P. Lee, P. Norreys, and M. Tatarakis, A study of picosecond laser–solid interactions up to 10^{19} W cm^{-2}, Phys. Plasmas **4**, 447 (1997).

[27] M. Cerchez, R. Jung, J. Osterholz, T. Toncian, O. Willi, P. Mulser, and H. Ruhl, Absorption of Ultrashort Laser Pulses in Strongly Overdense Targets, Phys. Rev. Lett. **100**, 245001 (2008).

[28] F. Brunel, Not-So-Resonant, Resonant Absorption, Phys. Rev. Lett. **59**, 52 (1987).

[29] S. A. Self, Focusing of spherical Gaussian beams, Appl. Opt. **22**, 658 (1983).

[30] B. Dromey, D. Adams, R. Hörlein, Y. Nomura, S. G. Rykovanov, D. C. Carroll, P. S. Foster, S. Kar, K. Markey, P. McKenna *et al.*, Diffraction-limited performance and focusing of high harmonics from relativistic plasmas, Nat. Phys. **5**, 146 (2009).

[31] C. Thaury, F. Quéré, J.-P. Geindre, A. Levy, T. Ceccotti, P. Monot, M. Bougeard, F. Réau, P. D'Oliveira, P. Audebert *et al.*, Plasma mirrors for ultrahigh-intensity optics, Nat. Phys. **3**, 424 (2007).

[32] E. Porat, A. Levanon, D. Roitman, I. Cohen, R. Louzon, and I. Pomerantz, Towards direct-laser-production of relativistic surface harmonics, in *Relativistic Plasma Waves and Particle Beams as Coherent and Incoherent Radiation Sources III*, edited by D. A. Jaroszynski and M. Hur (SPIE, Bellingham, 2019), Vol. 11036, p. 17.

[33] P. Tournois, Acousto-optic programmable dispersive filter for adaptive compensation of group delay time dispersion in laser systems, Opt. Commun. **140**, 245 (1997).

[34] E. Treacy, Optical pulse compression with diffraction gratings, IEEE J. Quantum Electron. **5**, 454 (1969).

[35] S. Kahaly, S. Monchocé, H. Vincenti, T. Dzelzainis, B. Dromey, M. Zepf, P. Martin, and F. Quéré, Direct Observation of Density-Gradient Effects in Harmonic Generation from Plasma Mirrors, Phys. Rev. Lett. **110**, 175001 (2013).

[36] O. Jahn, V. E. Leshchenko, P. Tzallas, A. Kessel, M. Krüger, A. Münzer, S. A. Trushin, G. D. Tsakiris, S. Kahaly, D. Kormin *et al.*, Towards intense isolated attosecond pulses from relativistic surface high harmonics, Optica **6**, 280 (2019).

[37] L. Chopineau, A. Leblanc, G. Blaclard, A. Denoeud, M. Thévenet, J. L. Vay, G. Bonnaud, P. Martin, H. Vincenti, and F. Quéré, Identification of Coupling Mechanisms between Ultraintense Laser Light and Dense Plasmas, Phys. Rev. X **9**, 011050 (2019).

[38] J. Geindre, P. Audebert, A. Rousse, F. Fallies, J. Gauthier, A. Mysyrowicz, A. Dos Santos, G. Hamoniaux, and A. Antonetti, Frequency-domain interferometer for measuring the phase and amplitude of a femtosecond pulse probing a laser-produced plasma, Opt. Lett. **19**, 1997 (1994).

[39] M. Bocoum, F. Böhle, A. Vernier, A. Jullien, J. Faure, and R. Lopez-Martens, Spatial-domain interferometer for measuring plasma mirror expansion, Opt. Lett. **40**, 3009 (2015).

[40] R. Trebino, K. W. DeLong, D. N. Fittinghoff, J. N. Sweetser, M. A. Krumbügel, B. A. Richman, and D. J. Kane, Measuring ultrashort laser pulses in the time-frequency domain using frequency-resolved optical gating, Rev. Sci. Instrum. **68**, 3277 (1997).

[41] T. Oksenhendler, S. Coudreau, N. Forget, V. Crozatier, S. Grabielle, R. Herzog, O. Gobert, and D. Kaplan, Self-referenced spectral interferometry, Appl. Phys. B **99**, 7 (2010).